Real time imaging of strain fields induced by the ferrite-to-austenite transformation in high purity iron

Nicolas Bruzy, Michel Coret, Bertrand Huneau, Laurent Stainier, Christophe Denoual, Marilyne Mondon, Guillaume Kermouche

Real time imaging of deformation induced by the ferrite-to-austenite transformation in high purity iron

N. Bruzy[1], M. Coret[1], B. Huneau[1], L. Stainier[1], C. Denoual[2], M. Mondon[3], and G. Kermouche[3]

[1]Ecole Centrale de Nantes, Université de Nantes, CNRS, UMR 6183 Institut de Recherche en Génie Civil et Mécanique (GeM), Nantes, France
[2]CEA, DAM, DIF, F-91297 Arpajon, France
[3]Mines de Saint-Etienne, Université de Lyon, CNRS, UMR 5307 Laboratoire Georges Friedel (LGF), Centre SMS, F-42023 Saint-Etienne, France

Abstract

During the ferrite-to-austenite transformation, the accommodation of the volume misfit between ferrite and austenite induces strain localization in both phases. A detailed understanding of this mechanism is a necessary step towards the improvement of thermomechanical treatments of iron alloys. Full-field measurements of displacement during heating of high purity iron samples are thoroughly post-processed to track the transformation *in situ*. They allow a fine characterization of the interaction between local plastic events and microstructure evolutions during the transformation. The deformation of austenite grains bears strong signatures in terms of orientation that can be used to monitor their individual growth in temperature. The parent phase acts as an elastoplastic matrix embedding an inclusion everywhere except at grain boundaries where additional localizations induced by crystal rotations precede the transformation interface.

Keywords Allotropic transformation; Microplasticity; Digital Image Correlation; Pure Iron

1 Introduction

The ferrite-to-austenite transformation that occurs in iron upon heating is marked by a period of coexistence of the two phases. Even under rapid heating rates, the temperature response of iron exhibits a thermal arrest at the transition temperature [1] (around $1180K$)

which is the signature of a first-order transient process during which the parent ferrite progressively transforms into the product austenite. More specifically, a candidate austenite nucleus forms by a random movement of atoms inside the ferrite crystalline structure. If its volume energy compensates the misfit energy of the created surfaces, an interface between the two phases is constituted and progresses in the material until the growing austenite grains impinge each other. The uncoordinated movement of atoms at the interface causes the initial crystal structure to be replaced by a new one. There is *a priori* no relation between either the mechanical state or the orientation of both structures, which explains why the ferrite-to-austenite transformation is classified as reconstructive in the sense of Buerger [2].

A corollary is that the transformation relaxes most (if not all) the deviatoric strain, and thus reduces the deformation to a spherical contribution related to the volume change between the two phases, around 2% [3]. This reconstruction must accommodate the misfit in the material for the strain to remain compatible. The aim of the present work is to observe *in situ* the formation of austenite grains inside a ferrite microstructure and to quantify locally the magnitude of the involved strain accommodation. Such an observation is challenging because among the equipments that permit to reach the ferrite-to-austenite transition temperature, none conciles sufficient space and time resolutions. Diffraction measurements, be it X-ray [4] or neutron [5] diffraction, give precise estimates of the local fraction of the different phases but cannot reach the scale of a few grains. Conversely, Electron BackScattered Diffraction (EBSD) is the preferred tool to investigate microstructural transformations. Yet, the scanning phase involved by the imaging process hinders real time observations, although efforts made in this direction by Ziljstra et al. [6] deserve to be noted. Halfway between the two, a recent experimental set-up [7] makes use of a high resolution camera to monitor phase changes at the mesoscale. Raw images are processed using the Digital Image Correlation (DIC) technique, which has emerged as the indisputable tool to investigate strain localizations in metallic materials [8]. It is here adapted to measure kinematic fields inside and around austenite grains growing in a ferrite matrix.

2 Methods

For this purpose, high purity iron samples (less than 15ppm of carbon) were prepared by cold crucible melting. The size of the zone of interest is $5mm$ x $8mm$, the thickness is $1mm$. A two-step thermomechanical treatment was used to coarsen the grain structure. The first step consisted in cold working followed by annealing at 800°C for two hours. The second step was a strain annealing treatment with a tension loading up to a longitudinal strain of 5.2% followed by annealing at 850°C for two hours. The resulting microstructure is equiaxed with a few grains in the zone of interest. EBSD mappings were performed at the beginning of the tests using a JEOL JSM-6500F at an acceleration voltage of $20kV$. The indexation step size is $5\mu m$. EBSD raw data were processed using the MTEX toolbox [9]. Six landmarks were made on the surface of the samples with a micro-indenter so that EBSD maps and image correlation results match together. When relevant, the grain boundaries of the initial microstructures are delimitated with red lines in the presented results. Two

samples are compared in this work: the first one is a reference sample, the second one was pre-deformed in tension after the grain coarsening treatment and before being put in the experimental equipment. The deformation of the second sample was performed in an MTS 100kN hydraulic tension machine up to a mean longitudinal strain (measured by DIC) in the zone of interest of 2%.

During phase transformation experiments, temperature is measured using a 2-colour pyrometer (SensorTherm METIS M322). The uncertainty in temperature is 0.3% of the measured values. Temperature is injected in a feedback loop for electric current control. The samples are heated by Joule effect at a constant rate of $30K.s^{-1}$. Meanwhile, the images of the surface are recorded during heating with a Prosilica GT6600 CCD camera (6576x4384px resolution). The first image is taken at a temperature of $673K$. The designed experimental set-up addresses the three main challenges that may arise when taking images under high temperature conditions:

- oxidation that deteriorates the surface of the sample. The testing box is vacuum purified before testing, then put in an argon atmosphere;
- heat haze effect, *i.e.* a distortion of the images induced by local modifications of the refractive index of the atmosphere. A constant argon flow is maintained during testing to circumvent this issue, in the fashion of the air knife system proposed by Novak and Zok [10].
- the deterioration of the images due to gray body radiation from the sample. The sample is lit using a blue light LED-ring and a passband filter in the blue wavelengths is put before the camera. This solution has been proven to be reliable in the domain of temperatures of interest (up to $1300K$) [11] and is frequently implemented for high temperature measurement applications [12, 13].

An alumina-based speckle pattern is deposited on the sample beforehand so that the images can be exploited to compute the displacement field $u(x, y)$ in the zone of interest. The DIC software UFreckles [14] is used. This software implements an FE-DIC algorithm, which means that the displacement field is discretised using finite element shape functions. The transformation gradient $\bar{\mathbf{F}}$ is then obtained by using the spatial derivatives of these shape functions. The Green-Lagrange strain tensor $\bar{\mathbf{E}}(x, y) = \frac{1}{2}\left(\bar{\mathbf{F}}(x, y)^T\bar{\mathbf{F}}(x, y) - \mathbf{I}\right)$ is finally computed. $\mathbf{I}$ is the two-dimensional second order identity tensor.

The bar notation recalls that computed tensors only contain in-plane components. The whole strain tensor cannot be reasonably extrapolated from this information. Several methods could have been considered to complement the in-plane data, in particular using a two-camera system [15] or an extensometer to monitor deformation in the thickness direction. However, none of these solutions could be implemented in the context of the presented experimental set-up. The fact that only three components of the Green-Lagrange tensor are known means that the present experimental procedure provides a projection of the Green-Lagrange strain tensor, implying that some transformation events will be missed if the transformation involves no deformation in the observed plane. That said, it should not be the case for the

ferrite-to-austenite transformation. Indeed, since it is a diffusive transformation, the involved deformation is expected to be mostly isotropic. Surface measurements should at least reflect volume change. In-plane data is thus considered relevant to study the phenomenology of the transformation.

A strain noise analysis is conducted in temperature in order to get an estimate for the order of magnitude of the error on strain components. A set of 10 stationary images are taken after the heating ramp during testing of the pre-deformed sample, at a constant temperature of $1273K$. A specific DIC computation is run on these images to determine the averaged strain components over the whole computation domain. The evaluated strain should normally be equal to zero in these conditions, the computed strain corresponds to measurement noise. The maximum deviations with respect to a zero noise situation are $0.5\text{x}10^{-4}$, $3.5\text{x}10^{-4}$ and $1.0\text{x}10^{-4}$ for the strain components $\bar{\mathbf{E}}_{xx}$, $\bar{\mathbf{E}}_{yy}$ and $\bar{\mathbf{E}}_{xy}$, respectively. This noise levels are between 1 and 5% of the considered strain values at the same temperature.

3 Results and discussion

3.1 Transformation onset

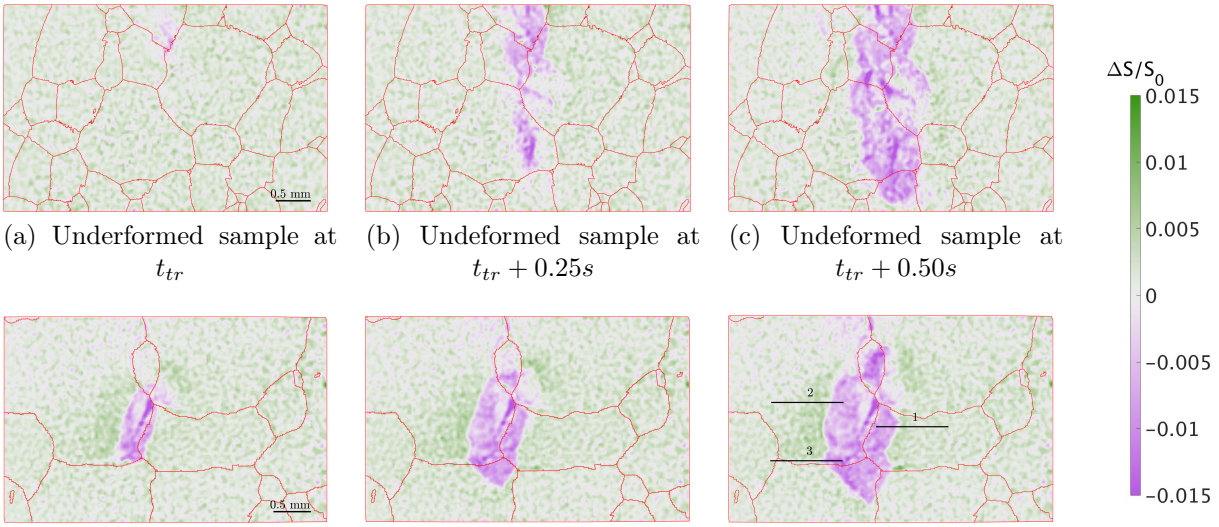

(a) Underformed sample at t_{tr}

(b) Undeformed sample at $t_{tr} + 0.25s$

(c) Undeformed sample at $t_{tr} + 0.50s$

(d) Predeformed sample at t_{tr}

(e) Predeformed sample at $t_{tr} + 0.25s$

(f) Predeformed sample at $t_{tr} + 0.50s$

Figure 1: Comparison of the ratio $\Delta S/S_0$ at the onset of transformation for the undeformed and pre-deformed samples. The initial microstructure is shown in red. The images are taken at the instant t_{tr} when $\Delta S/S_0$ is first inferior to 0.0 somewhere in the sample and at the instants $0.25s$ and $0.50s$ after. The three yellow lines in Figure 1f are used for the line plots presented in Figure 2.

Owing to the spherical nature of the transformation mechanical contribution, the most

reliable way to infer transformation events from the transformation gradient tensor $\mathbf{F}$ is the volume change. Following the considerations of the previous parts, the surface change $\Delta S/S_0 = \det(\bar{\mathbf{F}})$ is calculated. The underlying assumption is that since both dilatation and transformation contributions are isotropic, studying surface changes is sufficient to detect the ferrite-to-austenite transformation.

The volume reduction from ferrite to austenite implies that, in the conditions of the experiment, transformation has occurred if the ratio $\Delta S/S_0$ is negative. Figure 1 displays six maps of $\Delta S/S_0$ at the onset of the ferrite-to-austenite transformation for both the reference (Figures 1a, 1b and 1c) and the pre-deformed sample (Figures 1d, 1e and 1f).

An uncertainty remains on the location of transformation events as they could occur in the volume of the sample. However, it is clear from Figure 1 that the transformation initiates mainly at grain boundaries, as predicted by classical nucleation theory. A consequence of the pre-deformation is that nucleation tends to stay concentrated in one zone (Figure 1e) whereas several distinct nucleation events are seen in the case of the reference sample (Figure 1c). Indeed, the pre-deformation increases the amount of defects near grain boundaries by accentuating local mismatches [16], thus making heterogeneous nucleation sites even more energetically favourable. In what follows, results will only be presented for the pre-deformed sample for clarity. Similar conclusions can be drawn for the undeformed sample.

3.2 Mechanical accommodation of the transformation around the forming phase

Figure 1 is useful to identify the transformed region. It also shows a zone in expansion around this region, with values of the surface change well above 0.0. The ferrite matrix deforms as a consequence of the volume misfit between ferrite and austenite. Phase transformation by a reconstructive mechanism is believed to be accompanied by a purely isotropic deformation. To test this assumption and to complement the information given by the surface change, the Maximum Shear Strain quantity is defined as:

$$\mathrm{MSS} = \sqrt{\left(\frac{\bar{\mathbf{E}}_{xx} - \bar{\mathbf{E}}_{yy}}{2}\right)^2 + \bar{\mathbf{E}}_{xy}^2}. \tag{1}$$

This quantity has a deviatoric nature and is not altered by dilatation, which eliminates the effects of both thermal and phase change isotropic transformations. As such, it is a good way to characterize the elasto plastic activity taking place around the ferrite-to-austenite transformation, as exemplified in [7]. Line plots of the Maximum Shear Strain are presented in Figure 2. Surface change is superposed on these plots so that the $\Delta S/S_0 = 0$ criterion can be used to locate the ferrite/austenite interface (it is materialised by a green vertical line in Figure 2).

The first observation that can be drawn from this Figure is that shear strain magnitude near the ferrite/austenite interface is high, both in the initial and the final phase. The recorded shear strain levels seem to indicate a plastic activity in both ferrite and austenite grains. This means in particular that plasticity develops ahead of the transformation front.

Attempts to quantify the mechanical accommodation of austenite grains growth have been made in the frame of the study of the Greenwood and Johnson mechanism [17] for Transformation Induced Plasticity (TRIP). The mean response of the growing austenite grains is in a first approximation the solution of the Eshelby's problem of an inclusion growing in an infinite matrix of a different volume. This leads to a decrease in strain quantities in $\frac{1}{r^2}$ where r is the distance to the center of the inclusion. Both lines 1 and 2 are located far from initial ferrite grain boundaries, making it plausible that the austenite grains growing in these areas experience a homogenized medium, which falls in Eshelby's hypotheses. However, only shear strain along line 2 exhibits what could be a hyperbolic trend. More generally, there is a high heterogeneity in the strain field induced in ferrite by the accommodation of the transformation. This can be accounted for by the fact that austenite grains are not spherical. The transformed area even contains concavities, as highlighted by Figure 1f. Besides, this could be an effect of the discrepancies in the coherencies of the interfaces, an incoherent interface being likely to generate more plastic straining.

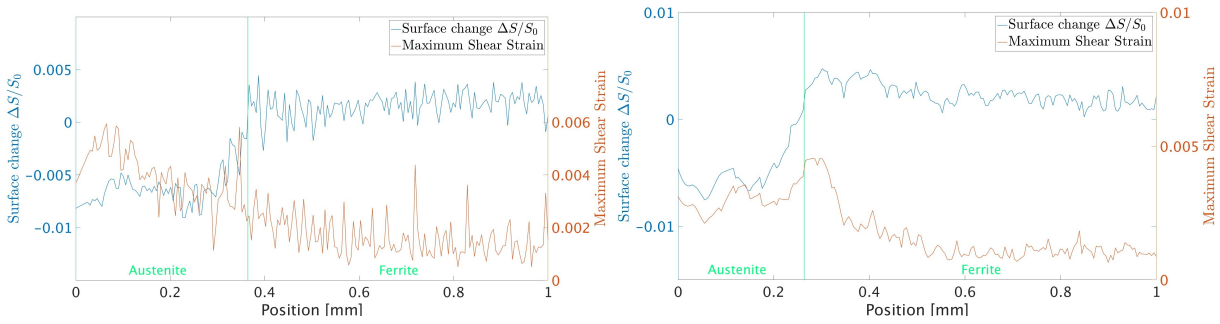

(a) Along line 1

(b) Along line 2

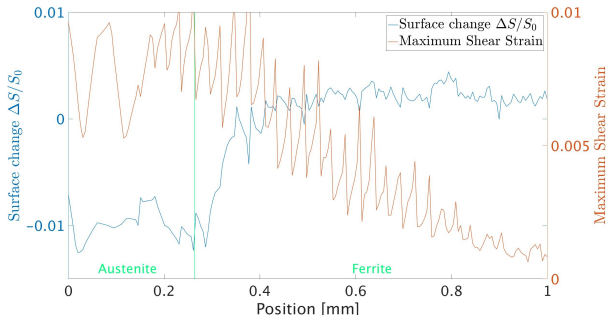

(c) Along line 3

Figure 2: Evolution of the surface change $\Delta S/S_0$ and the norm of the in-plane Green-Lagrange strain tensor $\bar{\mathbf{E}}$ across the ferrite-austenite interface (underlined by the vertical line) at the instant $t_{tr} + 0.75s$ at three different locations of the sample. Line numbering corresponds to the one presented in Figure 1f.

Near ferrite grain boundaries, such as is the case along line 3, the measured shear strain levels are even higher, even in the ferrite matrix. Such a trend is expected given the orientation misfits in these areas. A mapping of the maximum shear strain in presented in Figure 3.

Strain magnitudes are in accordance with Figure 2. The deviatoric strain tends to localize near grain boundaries where high crystal orientation incompatibilities are present. Crystal plasticity induces the development of a plastic zone that is located ahead of the transformed zone, *i.e.* there exists a plasticity that precedes the transformation in some specific zones of the sample. This means in particular that austenite grows in a matrix that has already been locally plastified by the transformation.

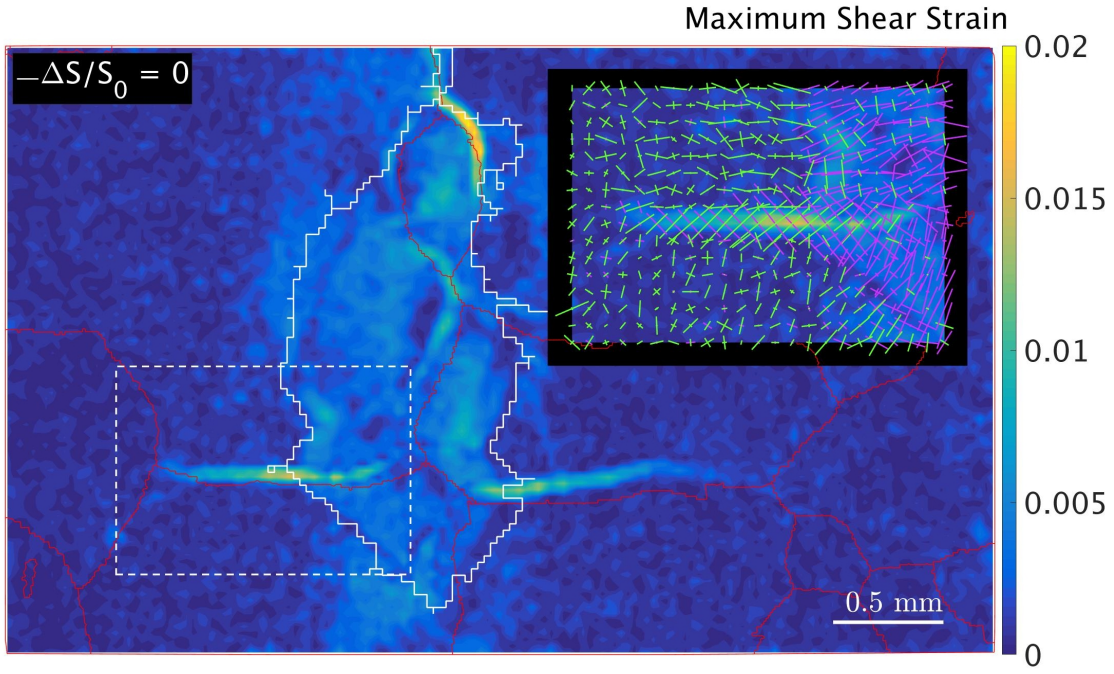

Figure 3: Mapping of the norm of the maximum shear strain at $t = t_{tr} + 0.5s$. Ferrite grain boundaries are shown in red. The solid white line is an isoline at 0.0 of the surface change, it delimitates the transformed region. A zoom is made on a grain boundaries region. In the zoomed box, strain eigenvectors directions are plotted with lines whose length is proportional to the deformation magnitude. Expansion states are shown in green, contraction states are shown in purple.

The eigenvectors of the in-plane Green-Lagrange strain tensor $\bar{\mathbf{E}}$ are calculated to characterize the direction of deformation near grain boundaries. Therefore, the eigenvectors directions obtained from this spectral analysis are plotted in the zoomed box in Figure 3. The lengths of the lines are proportional to the magnitude of the eigenvalues in absolute value and colors relate to their sign: expansion states are shown in green, contraction states are shown in purple. Near grain boundaries, the eigenvectors are inclined at approximately 45°with respect to the interface and both eigenvalues play similar roles, which is consistent with previous observations made during phase transformations [18] and highlights plastic shearing.

In the rest of the sample, however, there is always one eigenvalue whose magnitude is greater than the other. A contrast establishes between the top left-hand part of the zoomed

box where the direction associated with this eigenvector lie along the horizontal and the bottom left-hand part where no direction predominates. The interface between these two zones is the grain boundary. The formation of the new phase induces a heterogeneous mechanical accommodation in the ferrite grains. Plasticity concentrates in the vicinity of grain boundaries due to deformation jumps at the interface.

3.3 Deformation inside the forming phase

The closer one gets to the transformed region, the more ordered strain eigenvectors directions seem to be. For a given stress state, it is natural that the material response is driven by local crystal orientations. Yet strain eigenvectors directions are strikingly homogeneous inside the transformed region. Figure 4a shows a mapping of the inclination angles of the eigenvectors associated with the eigenvalues of $\bar{\mathbf{E}}$ in absolute value (*i.e.* the angle that the vector makes with the horizontal). Since the first or second are considered indistinctly to calculate this inclination, the angle is plotted modulo $\frac{\pi}{2}$.

No clear tendency emerges for the ferrite matrix. However, regions with similar strain eigenvectors directions can be detected in the transformed zone. One can emit the hypothesis that plotting these directions reveal the high-temperature microstructure. Following this idea, austenite grains were extracted from Figure 4a by performing successive thresholdings on inclination angle values. The evolution of two austenite grains is plotted in Figure 4b as a matter of illustration. Despite numerical artefacts due to the imprecisions in the identification of grain boundaries, the described behaviour is coherent with a nucleation and growth mechanism. There is first a rapid growth along a ferrite grain boundary, then the propagation of an interface between ferrite and austenite. It is worth noting that one can easily track austenite grains orientations even at high strain magnitudes.

4 Conclusion

In summary, the evolution of strain fields during phase transformations carry several layers of information about the mechanical response of iron to the formation of austenite upon heating. Three of them have been explored in the present study:

- the surface change $\Delta S/S_0$ provides a way to detect the onset of austenite formation. At the early stages of the transformation, classical results concerning the predominance of heterogeneous nucleation over homogeneous nucleation and the role of plastic deformation in making this difference more acute can be retrieved.

- the deviatoric part of the in-plane Green-Lagrange strain tensor highlights the microplasticity caused by the phase change both in the parent and product phases. This plasticity could precede the transformation interface.

- the eigenvectors of $\bar{\mathbf{E}}$ shed light on the out-of-isotropy aspects of the transformation. The tesselation of the deformation orientation map highlights a possible coupling between orientation selection and the overall strain.

The developed post-processing methodology constitutes in itself a promising tool to investigate the intricacy between inhomogeneous local mechanical states and nucleation-growth transformation mechanisms. Moreover, it could serve as a way to calibrate and/or validate modern numerical tools for the simulation of phase transformations at the mesoscale [19, 20, 21].

Acknowledgements

This work was partly supported by the SMICE project, which was funded by BPI France [grant number P113013-2660682].

Data availability

The raw/processed data required to reproduce these findings are available on request.

Bibliography

[1] J. Langner, J. Cahoon, Increase in the Alpha to Gamma Transformation Temperature of Pure Iron upon Very Rapid Heating, Metallurgical and Materials Transactions A 41 (2010) 1276–1283.

[2] M. Buerger, Crystallographic aspects of phase transformations, in: R. Smoluchowski, J. Mayer, W. Weyl (Eds.), Phase Transformations in Solids, John Wiley, 1951, pp. 183–209.

[3] H. Bhadeshia, R. Honeycombe, Chapter 1 - Iron and its interstitial solutions, in: H. Bhadeshia, R. Honeycombe (Eds.), Steels: Microstructure and Properties (Fourth Edition), Butterworth-Heinemann, fourth edition edition, 2017, pp. 1 – 22.

[4] V. I. Savran, S. E. Offerman, J. Sietsma, Austenite Nucleation and Growth Observed on the Level of Individual Grains by Three-Dimensional X-Ray Diffraction Microscopy, Metallurgical and Materials Transactions A 41 (2010) 583–591.

[5] P. Xu, Y. Tomota, P. Lukáš, O. Muránsky, Y. Adachi, Austenite-to-ferrite transformation in low alloy steels during thermomechanically controlled process studied by in situ neutron diffraction, Materials Science and Engineering: A 435-436 (2006) 46–53.

[6] G. Zijlstra, M. van Daalen, D. Vainchtein, V. Ocelík, J. De Hosson, Interphase boundary motion elucidated through in-situ high temperature electron back-scatter diffraction, Materials & Design 132 (2017) 138–147.

[7] N. Bruzy, M. Coret, B. Huneau, G. Kermouche, M. Mondon, E. Bertrand, L. Stainier, Mesoscopic strain fields measurement during the allotropic $\alpha - \gamma$ transformation in high purity iron, Experimental Mechanics 59 (2019) 1145–1157.

[8] B. Wattrisse, A. Chrysochoos, J.-M. Muracciole, M. Némoz-Gaillard, Kinematic manifestations of localisation phenomena in steels by digital image correlation, European Journal of Mechanics - A/Solids 20 (2001) 189 – 211.

[9] F. Bachmann, R. Hielscher, H. Schaeben, Grain detection from 2D and 3D EBSD data—specification of the MTEX algorithm, Ultramicroscopy 111 (2011) 1720 – 1733.

[10] M. D. Novak, F. W. Zok, High-temperature materials testing with full-field strain measurement: Experimental design and practice, Review of Scientific Instruments 82 (2011) 115101.

[11] B. Pan, D. Wu, Z. Wang, Y. Xia, High-temperature digital image correlation method for full-field deformation measurement at 1200 °c, Measurement Science and Technology 22 (2010) 015701.

[12] Y. Dong, H. Kakisawa, Y. Kagawa, Optical system for microscopic observation and strain measurement at high temperature, Measurement Science and Technology 25 (2013) 025002.

[13] G. Valeri, B. Koohbor, A. Kidane, M. A. Sutton, Determining the tensile response of materials at high temperature using dic and the virtual fields method, Optics and Lasers in Engineering 91 (2017) 53 – 61.

[14] J. Rethore, Ufreckles, 2018.

[15] S. Dilibal, H. Sehitoglu, R. Hamilton, H. Maier, Y. Chumlyakov, On the volume change in co–ni–al during pseudoelasticity, Materials Science and Engineering: A 528 (2011) 2875 – 2881.

[16] J. Sietsma, 14 - Nucleation and growth during the austenite-to-ferrite phase transformation in steels after plastic deformation, in: E. Pereloma, D. Edmonds (Eds.), Phase Transformations in Steels, volume 1, Woodhead Publishing, 2012, pp. 505–526.

[17] G. Greenwood, R. Johnson, The deformation of metals under small stresses during phase transformations, Proc. R. Soc. Lond. A 283 (1965).

[18] Y. Saotome, N. Iguchi, *In-situ* microstructural observations and micro-grid analyses of transfomation superplasticity in pure iron, Transactions of the Iron and Steel Institute of Japan 27 (1987) 696–704.

[19] K. Ammar, B. Appolaire, G. Cailletaud, S. Forest, Combining phase field approach and homogenization methods for modelling phase transformation in elastoplastic media, European Journal of Computational Mechanics 18 (2009) 485–523.

[20] F. Barbe, R. Quey, A numerical modelling of 3D polycrystal-to-polycrystal diffusive phase transformations involving crystal plasticity, International Journal of Plasticity 27 (2011) 823 – 840.

[21] T. Otsuka, R. Brenner, B. Bacroix, FFT-based modelling of transformation plasticity in polycrystalline materials during diffusive phase transformation, International Journal of Engineering Science 127 (2018) 92 – 113.

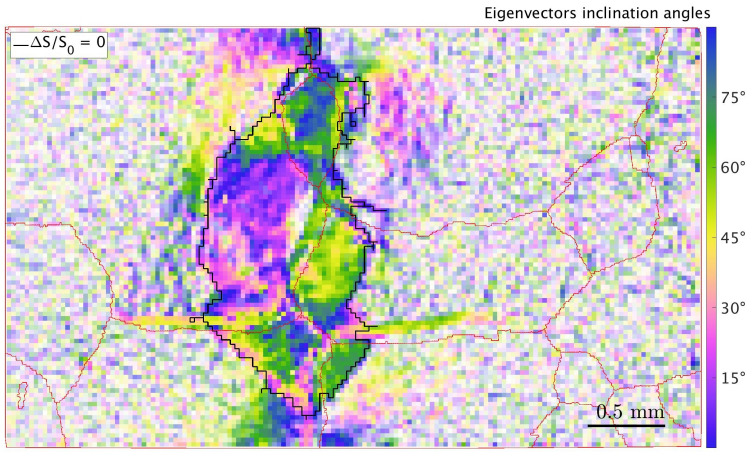

(a) Inclination angles of the eigenvectors of the tensor $\bar{\mathbf{E}}$ at $t = t_{tr} + 0.5s$. The transparency is adjusted to the magnitude of the associated eigenvalues. The solid black line is an isoline at 0.0 of the surface change, it delimitates the transformed region.

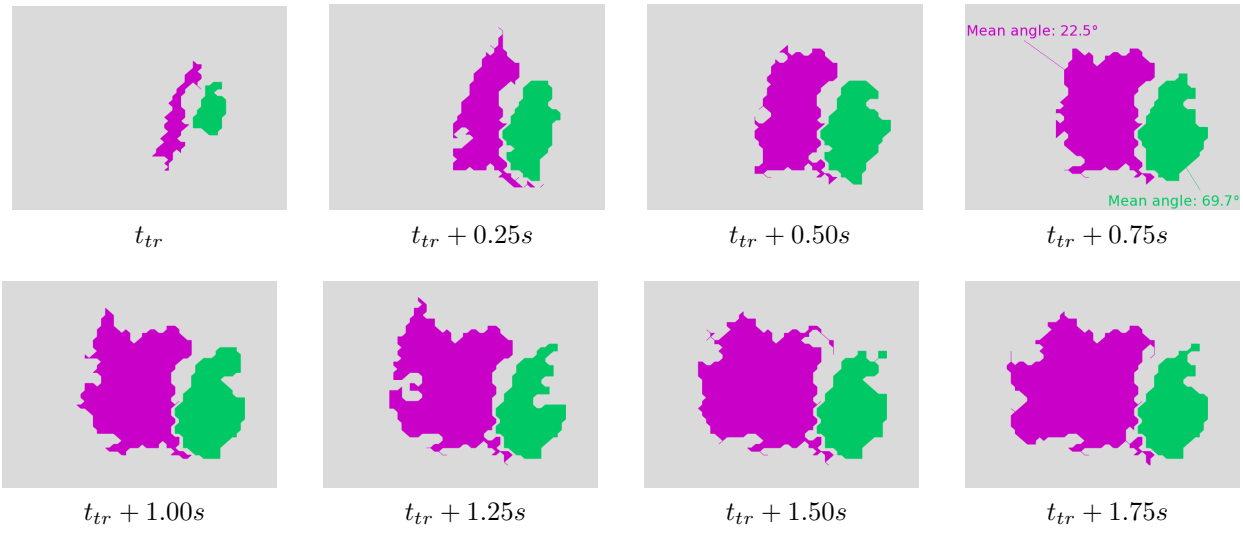

(b) Binary masks giving the evolution of the shape of two austenite grains.

Figure 4: Analysis of the inclination of strain eigenvectors inside growing austenite grains. The mapping at the top represents the inclinations of the eigenvectors of $\bar{\mathbf{E}}$ (the angles are folded between 0 and $\frac{\pi}{2}$). This representation is used to extract austenite grain boundaries. As a matter of illustration, the evolution of the shape of two austenite grains (labelled 1 and 2 in the top Figure) is shown at the bottom.